ACS OMEGA

Article

Cite This: ACS Omega 2018, 3, 14962−14972

http://pubs.acs.org/journal/acsodf

Capillary Interaction and Self-Assembly of Tilted Magnetic Ellipsoidal Particles at Liquid Interfaces

Bethany J. Newton,[†] Rizwaan Mohammed,[†,‡] Gary B. Davies,[§,⊥] Lorenzo Botto,[∥] and D. Martin A. Buzza[†,*]

[†]Nano3 Group, School of Mathematics & Physical Sciences, University of Hull, Hull HU6 7RX, U.K.

[‡]Clare College, Trinity Lane, Cambridge CB2 1TL, U.K.

[§]Institute for Computational Physics, Allmandring 3, 70569 Stuttgart, Germany

[∥]School of Engineering and Materials Science, Queen Mary, University of London, London E1 4NS, U.K.

ABSTRACT: Magnetic ellipsoidal particles adsorbed at a liquid interface provide exciting opportunities for creating switchable functional materials, where self-assembly can be switched on and off using an external field [Davies et al., *Adv. Mater.*, **2014**, *26*, 6715]. In order to gain a deeper understanding of this novel system in the presence of an external field, we study the capillary interaction and self-assembly of tilted ellipsoids using analytical theory and finite element simulations. We derive an analytical expression for the dipolar capillary interaction between tilted ellipsoids in elliptical polar coordinates, which exhibits a $1/r^2$ power law dependence in the far field (i.e., large particle separations r) and correctly captures the orientational dependence of the capillary interactions in the near field. Using this dipole potential and finite element simulations, we further analyze the energy landscape of particle clusters consisting of up to eight tilted ellipsoids in contact. For clusters of two particles, we find that the side-to-side configuration is stable, whereas the tip-to-tip configuration is unstable. However, for clusters of more than three particles, we find that circular loops of side-to-side particles become globally stable, whereas linear chains of side-to-side particles become metastable. Furthermore, the energy barrier for the linear-to-loop transition decreases with increasing particle number. Our results explain both thermodynamically and kinetically why tilted ellipsoids assemble side-to-side locally but have a strong tendency to form loops on larger length scales.

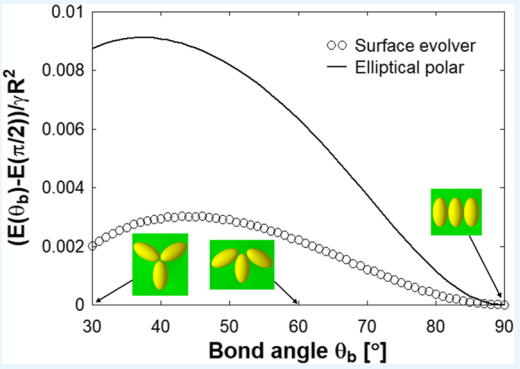

1. INTRODUCTION

Particles adsorbed at liquid interfaces occur in a wide range of soft matter systems from particle-stabilized emulsions and foams,[1] to membrane and interfacial proteins,[2] to functional surfaces for nanotechnology.[3,4] Most of the research in this area has focused on spherical or nearly spherical particles. However, with advancements in the synthesis of colloidal particles, particles with other shapes have received increasing attention over the last decade, including ellipsoids,[5−10] cylinders,[11−13] cubes,[14−17] and so forth. The behavior of such anisotropic particles at liquid interfaces is even richer than that of spherical particles for two reasons. First, anisotropic particles can adopt multiple orientations at the liquid interface.[11,13−17] Second, for non-neutrally wetting particles (i.e., contact angle $\theta_w \neq 90°$), the constant contact angle requirement at the three-phase contact line leads to significant deformations of the liquid meniscus around the anisotropic particles and hence strong capillary interactions between particles, even for particles on the micron scale where capillary forces due to gravity (i.e., so-called flotation forces) are negligible.[5−7,12,15−19]

These capillary interactions lead to a rich variety of self-assembled structures, a subject that is attracting growing interest, as evidenced by the number of recent review articles in this area.[20−22] By imposing external fields on particles at liquid interfaces such as electric,[23] magnetic,[4,24,25] or interfacial curvature,[26,27] it is possible to gain further control over the capillary interaction between particles and hence the self-assembly of particles at liquid interfaces, opening up exciting opportunities for creating switchable functional materials for photonic and sensing applications.[28] In this paper, we focus on controlling the self-assembly of anisotropic particles using magnetic fields. In particular, we focus on magnetic particles with ellipsoidal shape, arguably the simplest anisotropic shape one can consider. When such particles are adsorbed at a liquid interface, in the absence of an external magnetic field, the equilibrium orientation is the side-on state (i.e., long axis of the ellipsoids parallel to the liquid interface).[7] However, recent studies have shown that when an external field is applied

Received: July 30, 2018
Accepted: October 24, 2018
Published: November 6, 2018

DOI: 10.1021/acsomega.8b01818
ACS Omega 2018, 3, 14962−14972

perpendicular to the interface, it is possible to stabilize tilted orientations of the ellipsoidal particles, and above a critical field strength, the particles undergo an irreversible transition to the end-on state (i.e., long axis of ellipsoids perpendicular to the liquid interface).[8−10]

In a seminal study, Davies et al. showed using Lattice−Boltzmann (LB) simulations that the dipolar capillary attractions that exist between ellipsoidal particles in the tilted state can be used to create a simple switchable system where self-assembly can be turned on and off using an external field.[4] Specifically, Davies et al. considered an ensemble of micron-sized, neutrally wetting (θ_w = 90°) ellipsoidal particles at a liquid interface, where both monopolar capillary forces due to gravity and quadrupolar capillary deformations due to contact line undulations are negligible. In the absence of a magnetic field, the system is in the isotropic state where the side-on ellipsoids are randomly oriented within the interface. However, when an external field (below the critical field) is applied perpendicular to the interface, the dipolar capillary attractions cause the tilted ellipsoids to assemble side-to-side within the interface, forming so-called "capillary caterpillars". Davies et al. also observed that these capillary caterpillars had a strong tendency to form closed loops of different sizes, suggesting that dangling ends of the caterpillars are energetically unfavorable.

In order to gain a deeper understanding of the rich self-assembly behavior of this system, some of us performed a follow-up study of both the capillary interactions and self-assembly of tilted magnetic ellipsoids.[25] Using finite element simulations based on Surface Evolver,[29] we found that these capillary interactions conformed to the expected $1/r^2$ dipolar power law in the far field (i.e., large interparticle separations r) but deviated significantly from the dipolar power law in the near field (i.e., small r regime), presumably because of the importance of higher-order multipoles in this regime. We also found that the capillary attraction in the near field was stronger for particle pairs in the side-to-side configuration compared to the tip-to-tip configuration, consistent with the findings of ref 4 where the tilted ellipsoids preferred to assemble side-to-side. In addition, we investigated the self-assembly of between 3 and 12 tilted magnetic ellipsoids using LB simulations and found that these small clusters had a strong tendency to form closed loops, in excellent agreement with the observations of the larger-scale simulations in ref 4. However, the energy landscape for these small clusters was not mapped out as this information is not available from LB simulations.

An unexpected result in ref 25 is the fact that when the energy landscape for two tilted ellipsoids in contact was analyzed using Surface Evolver, it was found that while the side-to-side configuration was the global energy minimum, the tip-to-tip configuration was a locally stable metastable state with an energy barrier between the two states.[25] This result is in contrast to both experimental[30] and theoretical[18] studies of non-neutrally wetting side-on ellipsoidal particles, where the tip-to-tip configuration is found to be *unstable* and any particles approaching each other tip-to-tip tend to roll into the stable side-to-side configuration.

Clearly, despite the progress made in ref 25, there remain a number of important open questions regarding the self-assembly of tilted magnetic ellipsoids that require further investigation. The aim of this paper is to address these questions by performing a fuller analysis of the problem. First, we derive analytical expressions for the dipolar capillary interaction between tilted ellipsoids in elliptical polar coordinates. The advantage of using elliptical polar coordinates is that it allows us to effectively include higher-order circular polar multipoles in our pair potentials so that the resultant analytical expressions are accurate down to smaller r values.[7] Our analytical expression for the pair potentials also allows us to distinguish between particle pairs in the side-to-side compared to the tip-to-tip configuration. Second, we use both our derived pair potentials and Surface Evolver to map out the energy landscape of particle clusters containing two or more particles. Performing accurate Surface Evolver simulations for more than two particles is a nontrivial task, and as far as we are aware, our study represents the first time that the energy landscape for interfacial clusters containing more than two three-dimensional (3D) anisotropic particles has been mapped out in the literature. For two tilted ellipsoids in contact, we confirm that the side-to-side configuration is the global energy minimum. However, we also find that the tip-to-tip configuration is *unstable*. Interestingly, for clusters of three particles in contact, we find that circular loops of three side-to-side particles become metastable, whereas for four or more particles in contact, circular loops become globally stable, whereas linear chains of side-to-side configuration particles become metastable. Our study thus corrects an error we made in ref 25 about the stability of the tip-to-tip configuration for two-particle clusters but otherwise does not change the main conclusions of that paper. More importantly, the current study provides deeper mechanistic insights into the self-assembly results for tilted ellipsoids found in refs.[4,25]

Note that our theoretical approach neglects contact line pinning and hysteresis, although such phenomena could be present and important in real experimental systems. For example, recent experiments have shown that contact line pinning plays a dominant role in the adsorption of anisotropic particles at liquid interfaces.[31,32] However, theories neglecting pinning and contact line hysteresis have proven to serve as useful guidelines for both capillary interactions and self-assembly of anisotropic particles at liquid interfaces.[5,12,17,18] In addition, we believe that contact line pinning is more important in adsorption because the forces driving the motion are small (and become smaller and smaller as we approach the final equilibrium configuration of the particle), whereas pinning is comparatively less important in our system because we are applying a large external torque on each particle.

The rest of this paper is organized as follows. In Section 2, we discuss the configurational variables describing the collective behavior of multiple tilted ellipsoids and results for both the capillary interaction and self-assembly of clusters of two or more tilted ellipsoids. In Section 3, we summarize our key conclusions. In Section 4, we discuss the theoretical models used to analyze the behavior of the system, including details of the Surface Evolver model and the elliptical dipole potential.

2. RESULTS AND DISCUSSION

2.1. Configurational Space and Thermodynamics of the System. We consider magnetic ellipsoidal particles with semimajor axis length $L/2$, semiminor axis length R, and aspect ratio $\Lambda = L/2R$, which are adsorbed at an interface between two immiscible liquids. For convenience, we refer to the top liquid as "oil" and the bottom liquid as "water" in what follows. The particles have magnetic dipoles lying along their semimajor axis. An external magnetic field B is applied perpendicular to the oil/water interface, which interacts with

DOI: 10.1021/acsomega.8b01818
ACS Omega 2018, 3, 14962−14972

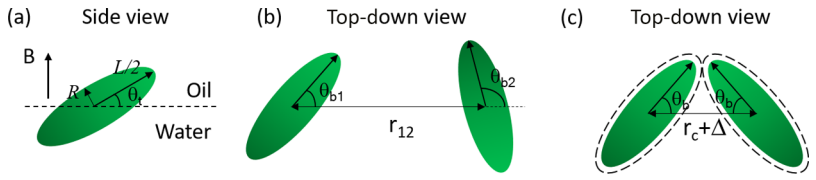

Figure 1. (a) Side view of single tilted ellipsoidal particle at an oil/water interface; (b) top-down view of a two-ellipsoidal particle system and variables used to describe the general in-plane configuration of the system; (c) top-down view of a mirror symmetric configuration of a two-ellipsoidal particle system where the particles are essentially in contact but with an exclusion zone of thickness $\Delta/2$ around each particle.

these magnetic dipoles and causes the particles to tilt such that their semimajor axes make an angle θ_t with respect to the unperturbed interface (Figure 1a). The value of the tilt angle θ_t depends on the magnetic field strength B.[8−10] In what follows, we parameterize the magnetic field strength by fixing θ_t to be at an appropriate value and B plays no further role in our discussion. For convenience, in what follows, we work with length and energy units, where $R = 1$ and the oil/water interfacial tension $\gamma_{ow} = 1$.

We consider micron-scale particles where monopolar capillary forces (i.e., flotation forces) are negligible. As we wish to focus on the effect of dipolar capillary forces in this paper, we assume that all ellipsoids are neutrally wetting (i.e., contact angle $\theta_w = 90°$) so that quadrupolar capillary interactions between particles are absent in the absence of a magnetic field. It is of course difficult to achieve perfect neutral wetting conditions in practice in an experimental system. However, the results in this paper should still apply to non-neutrally wetting tilted ellipsoids provided the tilt angle θ_t is high enough so that the amplitude of dipolar contact line undulations is greater than the amplitude of quadrupolar contact line undulations. In addition, as we shall see later, both dipolar and quadrupolar capillary forces tend to align the ellipsoidal particles in the same way, that is, into the side-to-side configuration. This again suggests that our results should apply to tilted ellipsoids that are not perfectly neutrally wetting.

For clusters of two tilted ellipsoids, translational and rotational invariance means that we require three variables to describe a general in-plane configuration of the system. We choose these variables to be the bond angles of each particle θ_{b1}, θ_{b2} and the center-to-center distance between the particles r_{12} as shown in Figure 1b. However, mapping out the entire energy landscape (i.e., minimum energy as a function of all the configurational variables) for even such a small system is already computationally very expensive. We therefore restrict ourselves to considering mirror symmetric configurations, that is, where $\theta_{b1} = 180° - \theta_{b2} = \theta_b$ (see Figure 1c), because dipolar capillary interaction energies are minimized for such configurations in polar coordinates.[25,39] In addition, because capillary interactions are attractive for mirror symmetric configurations, the energy of the cluster is minimized when the particles are in contact. We therefore set $r_{12} = r_c$, where r_c is the center-to-center distance between the particles in the mirror symmetric configuration when they are in contact. The distance r_c depends on both the bond angle θ_b and tilt angle θ_t of the two particles, and an analytical expression for $r_c(\theta_t,\theta_b)$ is given by eq A3 in Appendix A. Finally, to circumvent the numerical issues caused by simulating particles in contact, we define a thin exclusion zone of thickness $\Delta/2$ around each particle so that the minimum center-to-center distance between particles is $r_c + \Delta$ (Figure 1c). In all our calculations, we use $\Delta = 0.1R$. By varying Δ and extrapolating to $\Delta = 0$, we estimate that the energies obtained using $\Delta = 0.1R$ agree with the contact values to within 2%. Note that the two-particle configurations shown in Figure 1c are characterized only by the bond angle θ_b, with $\theta_b = 0°$ corresponding to the tip-to-tip configuration and $\theta_b = 90°$ corresponding to the side-to-side configuration (see Figure 4).

For clusters of three tilted ellipsoids, an even larger set of variables is required to describe the general in-plane configuration of the system, specifically the in-plane position vectors of particle centers and the bond angle of each particle (see Figure 2a). We can reduce the number of degrees of freedom from 9 to 6 by invoking translational and rotational invariance, but even so, a full exploration of the energy landscape of this system is computationally prohibitive. Following our discussion of two-particle clusters, we therefore restrict ourselves to considering configurations shown in Figure 2b, where nearest neighbors in the cluster have mirror symmetric configurations with a center-to-center distance of $r_c + \Delta$. Once again, such three-particle configurations are characterized only by the bond angle θ_b, with $\theta_b = 30°$ corresponding to a circular loop of three particles and $\theta_b = 90°$ corresponding to a linear chain of three side-to-side particles (see Figure 5). Finally, we can generalize the mirror symmetric configuration shown in Figure 2b to n particles, with the bond angle $\theta_b = 90° - 180°/n$ corresponding to a circular loop of n particles and $\theta_b = 90°$ corresponding to a linear chain of n particles (i.e., looped and circular capillary caterpillars, respectively).

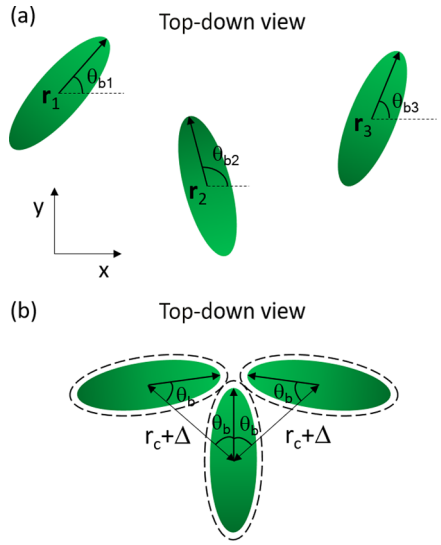

Figure 2. (a) Top-down view of a three-ellipsoidal particle system and variables used to describe the general in-plane configuration of the system; (b) top-down view of a mirror symmetric configuration of a three-ellipsoidal particle system, including an exclusion zone of thickness $\Delta/2$ around each particle.

DOI: 10.1021/acsomega.8b01818
ACS Omega 2018, 3, 14962−14972

For a given configuration of tilted ellipsoidal particles adsorbed at an oil/water interface, the total energy of the system is given by

$$E = \gamma_{ow}A_{ow} + \gamma_{po}A_{po} + \gamma_{pw}A_{pw} \quad (1)$$

where γ_{ij} and A_{ij} are the surface tension and area, respectively, of the i/j interface (i, j = o: oil, w: water, p: particle). Note that the above energy represents the interfacial energy of the system. We have not included the magnetic dipole−field interactions in the energy because these interactions are independent of the in-plane particle configurations and hence irrelevant to our discussions. We have also not included magnetic dipole−dipole interactions between particles because the primary focus of this paper is on the effect of capillary interactions on self-assembly. Using Young's equation $\cos\theta_w = (\gamma_{po} - \gamma_{pw})/\gamma_{ow}$, we can simplify eq 1 (up to a constant) to $E = \gamma_{ow}A_{ow} - \gamma_{ow}\cos\theta_w A_{pw}$. Finally, because we are only considering neutrally wetting particles in this paper where the contact angle $\theta_w = 90°$, the total energy of the system simplifies to

$$E = \gamma_{ow}A_{ow} \quad (2)$$

In what follows, we calculate the interfacial energy of the oil/water interface numerically using Surface Evolver (see Subsection 4.1) and analytically by modeling each tilted ellipsoid as an elliptical dipole (see Subsection 4.2).

2.2. Capillary Interaction. We first check the accuracy of the elliptical dipole potential given by eq 12. In Figure 3, we compare the capillary pair potential, that is, $\Delta E(r_{12}) = E(r_{12}) - E(\infty)$, as a function of the center-to-center distance r_{12} between two tilted ellipsoids with $\Lambda = 2$, $\theta_t = 5°$, calculated from eq 12 (solid curves) and from Surface Evolver simulations in ref 25 (data points), for the tip-to-tip configuration (blue) and the side-to-side configuration (red). For reference, we also show the asymptotic circular dipole potential given by eqs 13 and 14 (black dashed curve). For comparison in Figure 3, we used H_e as a fitting parameter and adjusted H_e so that the circular dipole potential (eq 13) matches the simulation data at large r_{12}. This procedure yields $H_e = 0.101R$, in good agreement with the value of $H_e = 0.087R$ obtained from our single particle simulations (see Subsection 4.2).

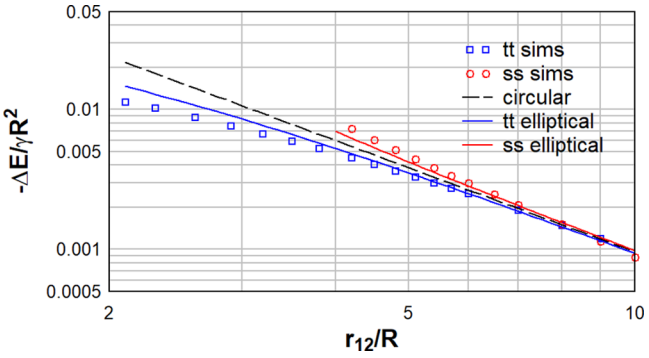

Figure 3. Capillary interaction energy as a function of the center-to-center distance r_{12} between two tilted ellipsoids with $\Lambda = 2$, $\theta_t = 5°$, calculated from the elliptical dipole potential (eq 12, solid curves) and from Surface Evolver simulations in ref 25 (data points), for the tip-to-tip configuration (blue) and the side-to-side configuration (red). For reference, we also show the asymptotic circular dipole potential (eq 13, black dashed curve). Note the sign of the vertical axis.

In the far field (large r_{12}), we see that the Surface Evolver data for both the tip-to-tip and side-to-side configurations approach the $1/r_{12}^2$ power law expected for dipoles. However, in the near field (small r_{12}), there are significant deviations of the Surface Evolver data from the circular dipolar potential because of the importance of higher-order circular polar multipoles.[25] Specifically, for all particle separations, the side-to-side configuration has a lower energy compared to the $1/r_{12}^2$ power law, whereas the tip-to-tip configuration has a higher energy (note the sign of the vertical axis in Figure 3).

Comparing now the elliptical dipole potential with the Surface Evolver results, we see that the elliptical potential (eq 12) correctly reproduces the $1/r_{12}^2$ power law in the far field. The elliptical potential also captures the correct sign for the near-field deviations from the circular dipolar potential for both the side-to-side and tip-to-tip configurations. However, the elliptical potential underestimates the magnitude of these deviations for both configurations, suggesting that higher-order elliptical multipoles are needed if we want to obtain quantitative agreement between analytical theory and numerical simulations. Nevertheless, the elliptical dipole potential (unlike the circular dipole potential) can correctly distinguish between the near-field interaction energies for different particle pair configurations and is therefore a useful tool for studying the energy landscape for particle clusters.

2.3. Energy Landscape. We next use both Surface Evolver and the elliptical dipole potential to analyze the energy landscape for the two-particle configurations shown in Figure 1c. In Figure 4, we plot the energy of two-particle clusters (relative to the side-to-side configuration $\theta_b = 90°$) as a function of the bond angle θ_b for $\Lambda = 2$, $\theta_t = 5°$, calculated from Surface Evolver (data points) and eq 15 with $H_e = 0.087R$ (solid line). From our Surface Evolver results, we find that the side-to-side configuration is the global energy minimum of the system, in agreement with the results of Davies et al.[25] However, unlike ref 25, we do not find a local minimum at $\theta_b = 0°$, that is, the tip-to-tip configuration is unstable rather than metastable. Our Surface Evolver results are corroborated by the elliptical polar results, which also show that the side-to-side configuration is globally stable, whereas the tip-to-tip configuration is unstable. The results in Figure 4 are also consistent with our expectation from simple electrostatics, where two in-plane electric dipoles in the tip-to-tip

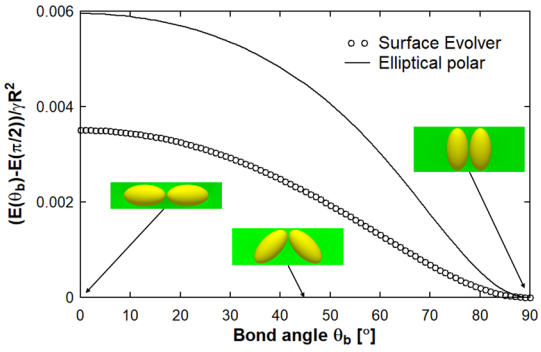

Figure 4. Capillary energy of two-particle clusters with mirror symmetric configurations shown in Figure 1c as a function of the bond angle θ_b for $\Lambda = 2$ and $\theta_t = 5°$, calculated from Surface Evolver (data points) and the elliptical dipole potential (solid line).

DOI: 10.1021/acsomega.8b01818
ACS Omega 2018, 3, 14962−14972

configuration with both dipoles pointing in the same direction (the analogue of the tip-to-tip configuration for capillary dipoles) are unstable and will ultimately collapse into an antiparallel side-to-side configuration (the analogue of the side-to-side configuration for capillary dipoles).

One possible reason for the error in ref 25 is that the relation between the center-to-center distance corresponding to contact and the bond and tilt angles is calculated via an iterative scheme in ref 25, while in this paper it is calculated exactly via an analytical formula (eq A3). From our experience, capillary forces are extremely sensitive to small variations in the minimum distance between particle surfaces so that even a small truncation error in ref 25 could have resulted in a (spurious) weak minimum in the potential. However, we emphasize that while Figure 4 corrects the error made in ref 25 about the stability of the tip-to-tip configuration, it does not change the main conclusion of that paper concerning the global stability of the side-to-side configuration. In particular, both our results here and those in ref 25 explain why tilted ellipsoids assemble side-to-side to form capillary caterpillars.

Interestingly, the energy landscape shown in Figure 4 is essentially the same as that for two-particle clusters of non-neutrally wetting side-on (i.e., nontilted) ellipsoidal particles, where the tip-to-tip configuration is also found to be unstable, and any particles approaching each other tip-to-tip tend to roll into the stable side-to-side configuration.[18,30] This suggests that if the tilted ellipsoids are not perfectly neutrally wetting, any quadrupolar capillary forces that are present in the system will reinforce the tendency of the dipolar forces to align the tilted ellipsoids side-to-side. We therefore expect that tilted ellipsoids that are not neutrally wetting will also form side-to-side capillary caterpillars.

We note that while the Surface Evolver and elliptical dipole results in Figure 4 agree with each other qualitatively, there are significant quantitative discrepancies between the two. This discrepancy can be attributed to the simplifying assumptions we made in our analytical treatment. First, only elliptical dipolar terms were included in our calculation, whereas Figure 3 suggests that higher-order multipoles should be included to obtain quantitatively accurate results. Second, our analytical calculations neglected nonlinear effects, such as large interfacial deformations and moving particle contact lines (see Subsection 4.2), which could be important for the small particle separations found in particle clusters. Notwithstanding this discrepancy, the qualitative agreement between our analytical and numerical results in Figure 4 confirms that the elliptical dipole potential captures the essential physics required to explore the energy landscape of ellipsoidal clusters.

We next use both Surface Evolver and the elliptical dipole potential to explore the energy landscape for the three-particle configurations shown in Figure 2b. In Figure 5, we plot the energy of three-particle clusters (relative to the side-to-side configuration $\theta_b = 90°$) as a function of the bond angle θ_b for $\Lambda = 2$, $\theta_t = 5°$, calculated from Surface Evolver (data points) and eq 16 with $H_e = 0.087R$ (solid line). Note that for three particles, θ_b goes from $\theta_b = 30°$ (circular loop of three side-to-side particles) to $\theta_b = 90°$ (linear chain of three side-to-side particles). From our Surface Evolver results, we find that the linear chain configuration continues to be the global energy minimum. However, the circular loop configuration is now metastable, and there is an energy barrier between the linear chain and circular loop states. These numerical results are corroborated by the elliptical polar results, which show the same qualitative behavior, that is, linear chains are globally stable, whereas circular loops are metastable.

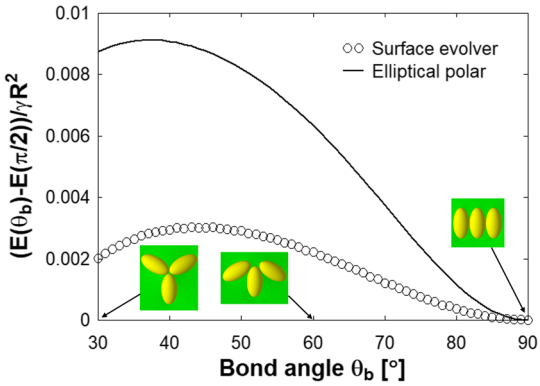

Figure 5. Capillary energy of three-particle clusters with mirror symmetric configurations shown in Figure 2b as a function of the bond angle θ_b for $\Lambda = 2$ and $\theta_t = 5°$, calculated from Surface Evolver (data points) and the elliptical dipole potential (solid line).

Interestingly, the discrepancy between the Surface Evolver and elliptical polar results for three-particle clusters (Figure 5) is significantly greater compared to that for two-particle clusters (Figure 4). The larger discrepancy may be due to many-body effects which were neglected in our analytical treatment, where we assumed that interactions were pairwise additive. However, it is known from the work of Fournier and Galatola on interfacial spherical clusters that such many-body effects can be significant for clusters.[33] However, the qualitative agreement between the analytical and numerical results in Figure 5 once again indicates that the elliptical dipole potential captures the essential physics required to explore the energy landscape of ellipsoidal clusters, even those containing more than two particles.

Comparing Figures 4 and 5, we see that the number of particles in the cluster n has a significant effect on the relative stability of the tip-to-tip and side-to-side configurations. In the final part of our discussion, we therefore extend our analysis to larger n values. In Figure 6, we show Surface Evolver results for the energy of mirror symmetric configurations containing n particles (i.e., the n particle analogues of Figure 2b) as a function of the bond angle θ_b, for $n = 2 \rightarrow 8$ ellipsoids with Λ

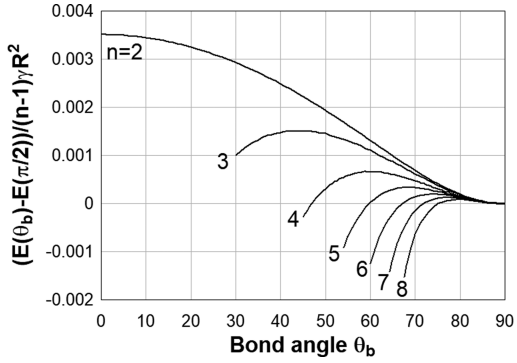

Figure 6. Capillary energy of n particle clusters with mirror symmetric configurations as a function of the bond angle θ_b for $\Lambda = 2$ and $\theta_t = 5°$, calculated from Surface Evolver for $n = 2 \rightarrow 8$. In order to directly compare energy curves for different n, each energy curve is normalized by $(n - 1)$, the number of nearest-neighbor capillary bonds in each cluster.

DOI: 10.1021/acsomega.8b01818
ACS Omega 2018, 3, 14962−14972

= 2, $\theta_t = 5°$. In order to directly compare the energy curves for different n, each curve is normalized by $(n - 1)$, the number of nearest-neighbor capillary bonds in each cluster. Note that θ_b goes from $\theta_b = 90° - 180°/n$ (circular loop) to $\theta_b = 90°$ (linear chain).

Interestingly, we see that for $n \geq 4$, circular loops become the global energy minimum, whereas linear chains become metastable. Indeed, the energy of circular loops relative to linear chains, E_{min}, decreases as we increase n (see Figure 7a).

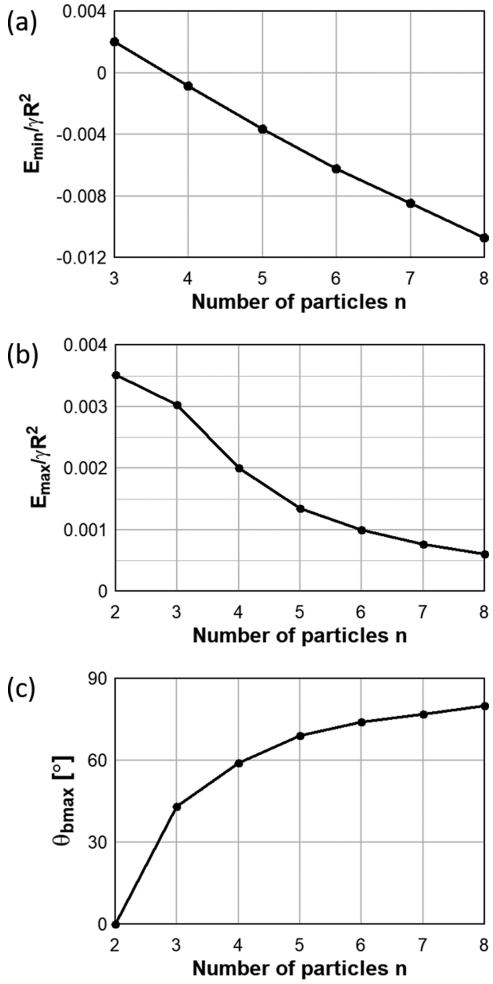

Figure 7. Key parameters characterizing the energy landscape shown in Figure 6 as a function of the number of particles in the cluster: (a) energy of circular loops relative to linear chains E_{min}; (b) energy barrier for the linear chain to loop transition E_{max}; and (c) bond angle of energy barrier θ_{bmax}.

These results suggest that dangling ends of linear chains are energetically unfavorable, providing a strong thermodynamic driving force for loop formation. In addition, the energy barrier for the linear chain to loop transition, E_{max}, also decreases with increasing n, tending to zero for large n (see Figure 7b). Furthermore, the bond angle at which the energy barrier occurs, θ_{bmax} increases with increasing n, tending toward 90° for large n (see Figure 7c). These results suggest that the kinetic barrier for loop formation decreases for large clusters. Together, the results in Figures 6 and 7 explain why the capillary caterpillars observed in refs[4,25] have such a strong tendency to form loops both thermodynamically and kinetically.

One of the striking features in Figure 6 is the collapse of the different energy curves onto a universal curve around $\theta_b = 90°$. This universal behavior can be understood as follows. The parabolic shape of the energy curves around $\theta_b = 90°$ suggests that the energetics in this regime is dominated by the elastic energy required to bend a linear capillary caterpillar.[18] Specifically, the curvature of each energy curve at $\theta_b = 90°$ is related to the flexural rigidity of the capillary caterpillar, which locally is due to the splaying of the ellipsoids on either side of a capillary bond.[18] Because the energy required to splay each capillary bond is independent of n, we expect all the energy curves to collapse onto a universal curve when they are normalized with respect to the number of capillary bonds.

We can rationalize the key features of the energy landscapes of the particle clusters by considering the micromechanics of bending the capillary caterpillars. Starting from the linear chain state at $\theta_b = 90°$, as we decrease the bond angle, the initial rise in energy is due to the elastic energy associated with bending the linear chain, as discussed earlier. However, as we decrease θ_b further, the chain ends eventually "see" each other. Because the capillary interactions between the chain ends are attractive, it is energetically favorable for the chain ends to be in contact to form the looped state. The energy curves therefore eventually deviate from the parabolic curve as θ_b is decreased, leading to an energy barrier between the linear and looped states. However, because the angular "distance" $90° - \theta_b$ before chain ends come into contact (or equivalently the degree to which the linear chains need to be bent locally) decreases as we increase n, the energy curves peel off from the parabolic regime at larger θ_b, leading to a larger θ_{bmax} and hence smaller E_{max} as we increase n.

We can also rationalize why E_{min} decreases as we increase n as follows. First, we note that E_{min} is essentially the bonding energy of chain ends, that is, the energy of chain ends when they are in contact relative to when they are not. Next, we see from Figure 4 that E_{min} depends on the bond angle θ_b of the chain ends when they are in contact. Specifically, because E_{min} is approximately the energy at θ_b relative to the energy at $\theta_b = 0°$ in Figure 4, E_{min} decreases as we increase θ_b. Finally, because the bond angle of chain ends when they are in contact θ_b increases as we increase n, this means that E_{min} decreases as we increase n.

Finally, we discuss the relevance of our calculations to experiment. Interestingly, both linear and looped caterpillars have been observed for nonmagnetic, non-neutrally wetting ellipsoidal particles in the "side-on" state.[18,34] With advancements in materials science, it is now possible to produce anisotropic particles with embedded ferromagnetic dipoles[35] or superparamagnetic dipoles.[36,37] We therefore expect that it should be possible to synthesize the required magnetic ellipsoidal particles and experimentally prepare the self-assembled structures predicted in this paper and in refs 4 and 25. Note also that for particles on the microscale, the energy barrier separating the different (locally or globally) stable states in Figure 6 can be very large (~several million kT). We therefore expect that the self-assembled structures formed by tilted ellipsoids may be easily trapped in metastable states. Indeed, it is observed experimentally that capillary interactions between anisotropic microparticles typically lead to kinetically trapped configurations.[19,38] Therefore, in order to prepare self-assembled tilted ellipsoids which are in the ground state, it may be necessary to apply external fields such as

DOI: 10.1021/acsomega.8b01818
ACS Omega 2018, 3, 14962−14972

interfacial shear or controlled sonication to help equilibrate the system.

3. CONCLUSIONS

In this paper, we have used both analytical theory and Surface Evolver numerical simulations to study the capillary interaction and self-assembly of magnetic ellipsoids, which are in the tilted state because of the application of an external field. Using a superposition approximation in the limit of small slopes, we first derived analytical expressions for the dipolar capillary interaction between tilted ellipsoids in elliptical polar coordinates. The derived elliptical dipole potential exhibits the correct $1/r^2$ power law dependence in the far field and correctly captures the orientational dependence of the capillary interactions in the near field. However, there was only semiquantitative agreement between the elliptical dipole potential and the numerical results in the near field, suggesting that higher-order elliptical multipoles need to be included in order to model the near-field interactions quantitatively. Nevertheless, the fact that the elliptical dipole potential can correctly distinguish between the near-field interaction energies for different particle pair configurations demonstrates that it is a useful tool for exploring the energy landscape of particle clusters.

Using the elliptical dipole potential and Surface Evolver simulations, we next analyzed the energy landscape of particle clusters consisting of up to eight tilted ellipsoids. For clusters of two particles, we found that the side-to-side configuration was stable, whereas the tip-to-tip configuration was unstable. This corrects an error we made in an earlier study[25] where we found that the tip-to-tip configuration was metastable for two-particle clusters. For clusters of three particles, we found that linear chains of three side-to-side particles continued to be the global energy minimum, but circular loops of three side-to-side ellipsoids became metastable. Finally, for clusters of four or more particles, circular loops became the global minimum, whereas linear chains became metastable. We also found that the energy barrier for the linear chain to loop transition decreased with increasing particle number. The key features of the energy landscape can be understood in terms of a competition between the elastic energy for bending linear chains and the bonding energy of chain ends. Our results provide a deeper mechanistic insight into the self-assembly of interfacial magnetic ellipsoids, which we hope will stimulate further experimental investigations of this system and open up exciting opportunities for creating responsive functional materials.

4. THEORETICAL METHODS

4.1. Surface Evolver. In Surface Evolver, the relevant interfaces in the system (in our case the oil/water interface only, see eq 2) are represented by a mesh of small triangles, and the resultant vertices are displaced to minimize the interfacial energy subject to appropriate constraints.[29] We define the $x-y$ plane of the lab frame to lie along the unperturbed oil/water interface and the z-axis to be perpendicular to the interface. Vertices on the three-phase contact line are required to satisfy the ellipsoid equation given by eq A1. The constant contact angle constraint is imposed by requiring the surface energies of the three interfaces meeting at the contact line to satisfy Young's equation. Specifically, we set $\gamma_{po} = \gamma_{pw} = 0$ and $\gamma_{ow} = 1$ to achieve $\theta_w = 90°$. Homogeneous Neumann boundary conditions are imposed at the outer boundary of the simulation box to ensure a flat interface far from the particle clusters. In order to compare our results to those in ref 25, we consider ellipsoids with aspect ratio $\Lambda = 2$ and tilt angle $\theta_t = 5°$. Depending on the number of particles simulated (2−8), we used simulation box sizes ranging from $10L \times 10L$ to $13L \times 13L$. The particle clusters were placed close to the center of the simulation box to minimize edge effects. For computational convenience and without loss of generality, the z-coordinate of all particle centers was fixed at zero, while the height of the oil/water interface was allowed to freely vary relative to the particles. In order to achieve good numerical accuracy, we used a mesh that had a higher level of refinement close to the particle. In the last stages of evolution, we changed the model type from linear to quadratic, which adds vertices at the midpoints of each edge, followed by further minimization which allows us to evaluate the areas and energy with high accuracy. Note that these additional refinements are critical because of the severe resolution requirements on the finite element mesh in the contact region for obtaining accurate and converged solutions in our calculations.

4.2. Capillary Interactions in Elliptical Coordinates. In addition to calculating the interfacial energies numerically using Surface Evolver, we also calculated these energies analytically by modeling each tilted ellipsoid as an elliptical dipole. For these calculations, we adopt a particle-centered elliptical coordinate system (s,t) which is related to the particle-centered Cartesian coordinate system (x,y) by the transformation

$$x = \alpha \cosh s \cos t$$
$$y = \alpha \sinh s \sin t \tag{3}$$

where the $t = 0$ line and the x-axis in eq 3 are assumed to lie along the semimajor axis of the particle. The coordinates (s,t) are analogous to the circular polar coordinates (r,θ), with $0 \leq s \leq \infty$ and $0 \leq \theta \leq 2\pi$. However, the advantage of the elliptical coordinates is that they take into account the aspect ratio of the particle. Specifically, the parameter α is a metric length scale that is adjusted so that the locus $s = s_0$ (an ellipse) coincides with the contact line of the particle. Using eq 3, it is easy to show that for ellipsoids with aspect ratio Λ[12]

$$\alpha = R\sqrt{\Lambda^2 - 1} \tag{4}$$

$$s_0 = \coth^{-1}(\Lambda) \tag{5}$$

Consider two identical tilted ellipsoids with bond angles θ_{b1} and θ_{b2} and center-to-center distance r_{12} as shown in Figure 1b. Let us denote the left and right particles in Figure 1b as particles 1 and 2, respectively, and introduce two elliptical coordinate systems, (s_1,t_1) and (s_2,t_2), centered around each of the two particle centers. The contact lines for particles 1 and 2 are located at $s = s_{01}$ and $s = s_{02}$, respectively. For tilted ellipsoids not acted upon by external forces, the leading order deformation of the oil/water interface is a capillary dipole.[7,12,39] Assuming the deformation of the oil/water interface is small, by solving the linearized Young−Laplace equation, one can show that the vertical displacement of the interface created by each particle is given in particle elliptical coordinates by[7]

$$h_1 = H_e\, e^{-(s_1 - s_{01})} \cos t_1 \tag{6}$$

DOI: 10.1021/acsomega.8b01818
ACS Omega 2018, 3, 14962−14972

$$h_2 = H_e\, e^{-(s_2 - s_{02})} \cos t_2 \tag{7}$$

where H_e is the amplitude of the contact line deformation around each particle, $s_{01} = s_{02} = s_0$, and s_0 is given by eq 5. Using the superposition approximation,[7,12,39,40] the total deformation of the interface due to both particles is given by

$$h = h_1 + h_2 \tag{8}$$

For small deformations, the interfacial energy of the system is (up to an unimportant constant)[12,39,40]

$$E(r_{12}) = \frac{\gamma_{ow}}{2}\int_{A_0} \nabla h \cdot \nabla h \, dA \tag{9}$$

where ∇h is the two-dimensional (2D) gradient of h and the integral is taken over the domain A_0, where the in-plane coordinates of the interface are external to the contact lines of each particle. On the other hand, the capillary pair potential, that is, $\Delta E(r_{12}) = E(r_{12}) - E(\infty)$, is given by[41]

$$\Delta E(r_{12}) = -2\gamma_{ow} \nabla h_1|_2 \cdot \mathbf{Q}_2 \tag{10}$$

where $\nabla h_1|_2$ is the 2D gradient of h_1 evaluated at the center of particle 2 and $\mathbf{Q}_2$ is the capillary dipole moment vector for particle 2 given by

$$\mathbf{Q}_2 = \oint h_2 \mathbf{n} \, dl \tag{11}$$

$\mathbf{n}$ is the outward pointing normal to the contact line of particle 2 (i.e., $s = s_{02}$) and dl is the length of a line element on the contact line. In Appendix B, we evaluate eq 10 analytically, and the final result for the elliptical dipole potential is

$$\begin{aligned}\Delta E(r_{12}, \theta_{b1}, \theta_{b2}) = -2\pi\gamma_{ow} H_e^{\,2}\, e^{-s_0} \\ \sinh(s_0)[\cos(\theta_{b1} - \theta_{b2}) G(s_1, t_1) \\ + \sin(\theta_{b1} - \theta_{b2}) L(s_1, t_1)]\end{aligned} \tag{12}$$

where s_0 is given by eq 5 and (s_1,t_1) are the elliptical coordinates of the center of particle 2. The expressions for the functions $G(s_1,t_1)$, $L(s_1,t_1)$ and the relationship between s_1, t_1 and r_{12}, θ_{b1}, and θ_{b2} are given in Appendix B.

For $r_{12} \to \infty$, the factor in square brackets on the right-hand side of eq 12 asymptotically approaches $-\frac{\alpha^2 \cos(\theta_{b1} + \theta_{b2})}{2r^2}$ so that the elliptical dipole potential asymptotically approaches the circular polar dipole potential[25,39,40]

$$\Delta E(r_{12}, \theta_{b1}, \theta_{b2}) = 2\pi\gamma_{ow} H_p^{\,2} \frac{R^2}{r_{12}^{\,2}} \cos(\theta_{b1} + \theta_{b2}) \tag{13}$$

where H_p is the effective amplitude of the contact line deformation in circular polars, that is, assuming the contact line to be at $r = R$. Comparing eqs 12 and 13, the amplitudes H_e and H_p are thus related to each other by

$$H_p = H_e \frac{\alpha}{R}\left(\frac{e^{s_0}\sinh(s_0)}{2}\right)^{1/2} \tag{14}$$

The amplitude H_e depends on the tilt angle θ_t. Consistent with the superposition approximation, we approximate $H_e(\theta_t)$ as the contact line deformation amplitude for an isolated tilted ellipsoid; this is an approximation because when two ellipsoids approach each other, the contact line on each particle may move in order to minimize the total interfacial energy of the system.[7] Using Surface Evolver, we obtain $H_e = 0.087R$ for a single ellipsoid with aspect ratio $\Lambda = 2$ and tilt angle $\theta_t = 5°$. In this paper, we use this value for H_e in our analytical calculations unless otherwise stated.

We can use the elliptical dipole potential given in eq 12 to analyze the energy landscape of the particle clusters considered in Subsection 2.1 analytically. For the two-particle clusters considered in Figure 1c, the interfacial energy of the cluster (up to an unimportant constant) as a function of the bond angle θ_b is given by

$$E(\theta_b) = \Delta E(r_c + \Delta, \theta_b, \pi - \theta_b) \tag{15}$$

where the expression for the contact distance r_c is given in eq A3. On the other hand, for the three-particle clusters considered in Figure 2b, assuming that interactions are pairwise additive and using simple geometry, the interfacial energy of the cluster as a function of θ_b is given by

$$\begin{aligned}E(\theta_b) = 2\Delta E(r_c + \Delta, \theta_b, \pi - \theta_b) \\ + \Delta E\left(2(r_c + \Delta)\sin\theta_b, 2\theta_b - \frac{\pi}{2}, \frac{3\pi}{2} - 2\theta_b\right)\end{aligned} \tag{16}$$

where the first term on the right-hand side represents the contributions from adjacent particle pairs in the cluster, whereas the second term is the contribution from the nonadjacent particle pair.

APPENDIX A

Derivation of the Contact Distance r_c

In this section, we derive an analytic expression for $r_c(\theta_t,\theta_b)$, the center-to-center distance between two contacting ellipsoidal particles with configuration given by Figure 1c (but with $\Delta = 0$) as a function of the tilt angle θ_t and bond angle θ_b. Let us define the $x-y$ plane of the lab frame to lie along the unperturbed oil/water interface and the z-axis to be perpendicular to the interface. For definiteness, let us focus on the particle on the left in Figure 1c and define the positive x-axis to point to the right and the positive y-axis to point vertically upward. The surface of this particle is described by the ellipsoid equation

$$f(x, y, z) = \left(\frac{2x''}{L}\right)^2 + \left(\frac{y''}{R}\right)^2 + \left(\frac{z''}{R}\right)^2 = 1 \tag{A1}$$

where x'', y'', z'' are the particle frame coordinates with the origin at the particle center, x'' aligned along the semimajor axis and y'', z'' along the semiminor axis. Denoting the coordinate of the particle center in the lab frame as $\mathbf{R} = (X, Y, Z)$, the particle coordinates (x'', y'', z'') are related to the lab coordinates (x, y, z) by the transformation

$$\begin{pmatrix} x'' \\ y'' \\ z'' \end{pmatrix} = \begin{pmatrix} \cos\theta_t & 0 & -\sin\theta_t \\ 0 & 1 & 0 \\ \sin\theta_t & 0 & \cos\theta_t \end{pmatrix} \begin{pmatrix} \cos\theta_b & \sin\theta_b & 0 \\ -\sin\theta_b & \cos\theta_b & 0 \\ 0 & 0 & 1 \end{pmatrix} \begin{pmatrix} x - X \\ y - Y \\ z - Z \end{pmatrix} \tag{A2}$$

that is, to obtain the particle frame, the lab frame is first translated by $\mathbf{R}$ so that the origin is at the particle center, rotated about the z-axis by the bond angle θ_b, and then rotated about the resultant y'-axis by the tilt angle θ_t.

The surface normal vector for the ellipsoid is given by ∇f, where $f(x,y,z)$ is the function given by eq A1 and ∇ is the 3D grad operator in the lab frame. At the point of contact between

DOI: 10.1021/acsomega.8b01818
ACS Omega 2018, 3, 14962−14972

the two particles in Figure 1c, the y and z components of ∇f are zero, that is, $\frac{\partial f}{\partial y} = \frac{\partial f}{\partial z} = 0$. Together with eq A1, this gives us three simultaneous equations which we can solve to find the coordinates of the contact point. The contact distance r_c is then just twice the x contact coordinate. The final result is

$$r_c(\theta_t, \theta_b) = 2R\{\Lambda^2(\cos\theta_b)^2(\cos\theta_t)^2 + (\cos\theta_b)^4(\sin\theta_t)^2 + (\sin\theta_b)^2[(\cos\theta_t)^2 + \frac{1}{2}(\sin\theta_t)^2(3 + \cos 2\theta_b)]\}^{1/2} \tag{A3}$$

APPENDIX B

Derivation of the Elliptical Dipole Potential

In this section, we evaluate eq 10 analytically to find the capillary pair potential ΔE as a function of the particle separation r_{12} and bond angles θ_{b1} and θ_{b2} shown in Figure 1b. To simplify our discussion, we first rewrite the interfacial deformation due to each particle h_1, h_2 as

$$h_1 = \hat{H}_e\, e^{-s_1}\cos(t_1) \tag{B1}$$

$$h_2 = \hat{H}_e\, e^{-s_2}\cos(t_2) \tag{B2}$$

Comparing eqs 6 and 7 with eqs B1 and B2, the amplitudes in both sets of equations are related to each other by

$$\hat{H}_e = H_e\, e^{s_0} \tag{B3}$$

where s_0 is given by eq 5. In elliptic coordinates, the normal to the reference contact line (s_0,t)in eq 11 is

$$n = \frac{1}{\sqrt{\sinh^2 s_0 + \sin^2 t}}\begin{pmatrix}\sinh s_0 \cos t\\ \cosh s_0 \sin t\end{pmatrix} \tag{B4}$$

and $dl = \alpha\sqrt{\sinh^2 s_0 + \sin^2 t}\, dt$.

To simplify the calculation of eq 10, we first write the gradient and the dipole moment vector in the frames of reference (x_1',y_1') (x_2',y_2') aligned with the major axis of each particle and then rotate the vectors in a frame aligned with the line joining the centers of the two particles. The rotated frames (x_1,y_1) and (x_2,y_2) have centers separated by a distance r_{12}. Their axes x_1 and x_2 are parallel to each other, so the dot product in eq 10 can be obtained readily. The frame (x_1',y_1') is obtained from (x_1,y_1) upon a counterclockwise rotation by an angle θ_{b1}, and similarly (x_2',y_2') is obtained from (x_2,y_2) upon a counterclockwise rotation by an angle θ_{b2}.

In the (x_1',y_1')frame, the components of the gradient are

$$\partial_{x_1'}h_1 = \partial_{s_1}h_1\partial_{x_1'}s_1 + \partial_{t_1}h_1\partial_{x_1'}t_1 \tag{B5}$$

and

$$\partial_{y_1'}h_1 = \partial_{s_1}h_1\partial_{y_1'}s_1 + \partial_{t_1}h_1\partial_{y_1'}t_1 \tag{B6}$$

where $\partial_{x_1'}s_1$, $\partial_{x_1'}t_1$, $\partial_{y_1'}s_1$, $\partial_{y_1'}t_1$ can be obtained by implicit differentiation of the mapping between Cartesian and elliptic coordinates given by eq 3, namely,

$$x_1' = \alpha\cosh s_1\cos t_1 \tag{B7}$$

$$y_1' = \alpha\sinh s_1\sin t_1 \tag{B8}$$

In the (x_1,y_1) frame, the components of the gradient are

$$\nabla h_1 = \begin{pmatrix}\cos\theta_{b1} & -\sin\theta_{b1}\\ \sin\theta_{b1} & \cos\theta_{b1}\end{pmatrix}\begin{pmatrix}\partial_{x_1'}h_1\\ \partial_{y_1'}h_1\end{pmatrix} = \begin{pmatrix}\cos\theta_{b1}\partial_{x_1'}h_1 - \sin\theta_{b1}\partial_{y_1'}h_1\\ \sin\theta_{b1}\partial_{x_1'}h_1 + \cos\theta_{b1}\partial_{y_1'}h_1\end{pmatrix} \tag{B9}$$

In the (x_2',y_2') frame, the components of the dipole vector are

$$Q_{x_2'} = \alpha\tilde{H}_2\, e^{-s_{02}}\sinh s_{02}\int_{t_2=0}^{2\pi}\cos^2 t_2\, dt_2 = \pi\alpha\tilde{H}_2\, e^{-s_{02}}\sinh s_{02} \tag{B10}$$

and

$$Q_{y_2'} = 0 \tag{B11}$$

In the (x_2,y_2) frame, the corresponding components are

$$\begin{pmatrix}Q_{2x}\\ Q_{2y}\end{pmatrix} = \begin{pmatrix}\cos\theta_{b2} & -\sin\theta_{b2}\\ \sin\theta_{b2} & \cos\theta_{b2}\end{pmatrix}\begin{pmatrix}Q_{x_2'}\\ 0\end{pmatrix} = Q_{x_2'}\begin{pmatrix}\cos\theta_{b2}\\ \sin\theta_{b2}\end{pmatrix} \tag{B12}$$

Carrying out the dot product, the capillary energy can be written as

$$\Delta E = -2\gamma Q_{x_2'}[\cos(\theta_{b1} - \theta_{b2})\partial_{x_1'}h_1 + \sin(\theta_{b1} - \theta_{b2})\partial_{y_1'}h_1] \tag{B13}$$

where

$$\partial_{x_1'}h_1 = \frac{\tilde{H}_1\, e^{-s_1}(\sin t_1\tan t_1 - \cos t_1\tanh s_1)}{\alpha\cosh s_1\cos t_1(\tanh^2 s_1 + \tan^2 t_1)} \tag{B14}$$

and

$$\partial_{y_1'}h_1 = -\frac{\tilde{H}_1\, e^{-s_1}(\sin t_1\tanh s_1 + \cos t_1\tan t_1)}{\alpha\cosh s_1\cos t_1(\tanh^2 s_1 + \tan^2 t_1)} \tag{B15}$$

or, more compactly, as

$$\Delta E = -2\pi\gamma\tilde{H}_1\tilde{H}_2\, e^{-s_{02}}\sinh s_{02}[\cos(\theta_{b1} - \theta_{b2})G(s_1, t_1) + \sin(\theta_{b1} - \theta_{b2})L(s_1, t_1)] \tag{B16}$$

where

$$G(s_1, t_1) = \frac{e^{-s_1}(\sin t_1\tan t_1 - \cos t_1\tanh s_1)}{\cosh s_1\cos t_1(\tanh^2 s_1 + \tan^2 t_1)} \tag{B17}$$

and

$$L(s_1, t_1) = \frac{e^{-s_1}(\sin t_1\tanh s_1 + \cos t_1\tan t_1)}{\cosh s_1\cos t_1(\tanh^2 s_1 + \tan^2 t_1)}. \tag{B18}$$

Inserting eq B3 and $s_{02} = s_0$ into eq B16, we obtain eq 12. Finally, we need to express the elliptic coordinates (s_1,t_1) of the center of particle 2 as a function of r_{12}, θ_{b1}, and θ_{b2}. The relationship between these two sets of coordinates can be obtained by noting that

$$r_{12}\cos\theta_{b1} = \alpha\cosh s_1\cos t_1 \tag{B19}$$

$$r_{12}\sin\theta_{b1} = \alpha\sinh s_1\sin t_1 \tag{B20}$$

Using these expressions, it is easy to see that t_1 can be first calculated from

DOI: 10.1021/acsomega.8b01818
ACS Omega 2018, 3, 14962−14972

$$\sin t_1 = \pm\left(\frac{1 - (r_{12}/\alpha)^2 + \sqrt{((r_{12}/\alpha)^2 - 1)^2 + 4(r_{12}/\alpha)^2 \sin^2\theta_{b1}}}{2}\right)^{1/2} \quad \text{(B21)}$$

and then s_1 is calculated from

$$s_1 = \tanh^{-1}\frac{\tan\theta_{b1}}{\tan t_1} \quad \text{(B22)}$$

In eq B21, the minus sign is for $0 \le \theta_{b1} \le \pi$ and the plus sign is for $\theta_{b1} < 0$ or $\theta_{b1} > \pi$.

AUTHOR INFORMATION

Corresponding Author

*E-mail: d.m.buzza@hull.ac.uk (D.M.A.B.).

ORCID

D. Martin A. Buzza: 0000-0002-9728-7858

Present Address

⊥St Paul's Girls' School, Brook Green, London, W6 7BS, UK.

Notes

The authors declare no competing financial interest.

ACKNOWLEDGMENTS

B.J.N. gratefully acknowledges the financial support from the University of Hull, the Joseph and Annie Cattle Trust, the Elizabeth Walker Foundation, and the Ann Watson's Trust for this work.

REFERENCES

(1) Binks, B. P. Particles as surfactants - similarities and differences. *Curr. Opin. Colloid Interface Sci.* **2002**, *7*, 21−41.

(2) Bromley, K. M.; Morris, R. J.; Hobley, L.; Brandani, G.; Gillespie, R. M. C.; McCluskey, M.; Zachariae, U.; Marenduzzo, D.; Stanley-Wall, N. R.; MacPhee, C. E. Interfacial self-assembly of a bacterial hydrophobin. *Proc. Natl. Acad. Sci. U.S.A.* **2015**, *112*, 5419−5424.

(3) Law, A. D.; Auriol, M.; Smith, D.; Horozov, T. S.; Buzza, D. M. A. Self-assembly of two-dimensional colloidal clusters by tuning the hydrophobicity, composition, and packing geometry. *Phys. Rev. Lett.* **2013**, *110*, 138301.

(4) Davies, G. B.; Krüger, T.; Coveney, P. V.; Harting, J.; Bresme, F. Assembling ellipsoidal particles at fluid interfaces using switchable dipolar capillary interactions. *Adv. Mater.* **2014**, *26*, 6715−6719.

(5) Loudet, J. C.; Alsayed, A. M.; Zhang, J.; Yodh, A. G. Capillary interactions between anisotropic colloidal particles. *Phys. Rev. Lett.* **2005**, *94*, 018301.

(6) Loudet, J. C.; Yodh, A. G.; Pouligny, B. Wetting and contact lines of micrometer-sized ellipsoids. *Phys. Rev. Lett.* **2006**, *97*, 018304.

(7) Lehle, H.; Noruzifar, E.; Oettel, M. Ellipsoidal particles and fluid interfaces. *Eur. Phys. J. E* **2008**, *26*, 151−160.

(8) Bresme, F.; Faraudo, J. Orientational transitions of anisotropic nanoparticles at liquid-liquid interfaces. *J. Phys. Condens. Matter* **2007**, *19*, 375110.

(9) Davies, G. B.; Krüger, T.; Coveney, P. V.; Harting, J.; Bresme, F. Interface deformations affect the orientation transition of magnetic ellipsoidal particle adsorbed at fluid-fluid interfaces. *Soft Matter* **2014**, *10*, 6742−6748.

(10) Newton, B. J.; Brakke, K. A.; Buzza, D. M. A. Influence of magnetic field on the orientation of anisotropic magnetic particles at liquid interfaces. *Phys. Chem. Chem. Phys.* **2014**, *16*, 26051−26058.

(11) Lewandowski, E. P.; Searson, P. C.; Stebe, K. J. Orientation of a nanocylinder at a fluid interface. *J. Phys. Chem. B* **2006**, *110*, 4283−4290.

(12) Lewandowski, E. P.; Cavallaro, M., Jr.; Botto, L.; Bernate, J. C.; Garbin, V.; Stebe, K. J. Orientation and self-assembly of cylindrical particles by anisotropic interactions. *Langmuir* **2010**, *26*, 15142−15154.

(13) Newton, B. J.; Buzza, D. M. A. Magnetic cylindrical colloids at liquid interfaces exhibit non-volatile switching of their orientation in an external field. *Soft Matter* **2016**, *12*, 5285−5296.

(14) Morris, G.; Neethling, S. J.; Cilliers, J. J. A model for investigating the behaviour of non-spherical particles at interfaces. *J. Colloid Interface Sci.* **2011**, *354*, 380−385.

(15) Dasgupta, S.; Katava, M.; Faraj, M.; Auth, T.; Gompper, G. Capillary assembly of microscale ellipsoidal, cuboidal, and speherical particles and interfaces. *Langmuir* **2014**, *30*, 11873−11882.

(16) Soligno, G.; Dijkstra, M.; van Roij, R. Self-assembly of cubes into 2D hexagonal and honeycomb lattices by hexapolar capillary interactions. *Phys. Rev. Lett.* **2016**, *116*, 258001.

(17) Anjali, T. G.; Basavaraj, M. G. Shape-induced deformation, capillary bridging, and self-assembly of cuboids at the fluid-fluid interface. *Langmuir* **2017**, *33*, 791−801.

(18) Botto, L.; Yao, L.; Leheny, R. L.; Stebe, K. J. Capillary bond between rod-like particles and the micromechanics of particle-laden interfaces. *Soft Matter* **2012**, *8*, 4971.

(19) Botto, L.; Lewandowski, E. P.; Cavallaro, M.; Stebe, K. J. Capillary interactions between anisotropic particles. *Soft Matter* **2012**, *8*, 9957.

(20) Bleibel, J.; Domínguez, A.; Oettel, M. Colloidal particles at fluid interfaces: Effective interactions, dynamics and a gravitationlike instability. *Eur. Phys. J. Spec. Top.* **2013**, *222*, 3071−3087.

(21) Dasgupta, S.; Auth, T.; Gompper, G. Nano- and microparticles at fluid and biological interfaces. *J. Phys.: Condens. Matter* **2017**, *29*, 373003.

(22) Liu, I. B.; Sharifi-Mood, N.; Stebe, K. J. Capillary assembly of colloids: interactions on planar and curved interfaces. *Annu. Rev. Condens. Matter Phys.* **2018**, *9*, 283−305.

(23) Mittal, M.; Furst, E. M. Electric fielddirected convective assembly of ellipsoidal colloidal particles to create optically and mechanically anisotropic thin films. *Adv. Funct. Mater.* **2009**, *19*, 3271−3278.

(24) Lumay, G.; Obara, N.; Weyer, F.; Vandewalle, N. Self-assembled magnetocapillary swimmers. *Soft Matter* **2013**, *9*, 2420.

(25) Davies, G. B.; Botto, L. Dipolar capillary interactions between tilted ellipsoidal particles adsorbed at fluid-fluid interfaces. *Soft Matter* **2015**, *11*, 7976.

(26) Cavallaro, M.; Botto, L.; Lewandowski, E. P.; Wang, M.; Stebe, K. J. Curvature-driven capillary migration and assembly of rod-like particles. *Proc. Natl. Acad. Sci. U.S.A.* **2011**, *108*, 20923−20928.

(27) Ershov, D.; Sprakel, J.; Appel, J.; Cohen Stuart, M. A.; van der Gucht, J. Capillarity-induced ordering of spherical colloids on an interface with anisotropic curvature. *Proc. Natl. Acad. Sci. U.S.A.* **2013**, *110*, 9220−9224.

(28) Kim, S.-H.; Lee, S. Y.; Yang, S.-M.; Yi, G.-R. Self-assembled colloidal structures for photonics. *NPG Asia Mater.* **2011**, *3*, 25−33.

(29) Brakke, K. A. The Surface Evolver. *Exp. Math.* **1992**, *1*, 141−165.

(30) Loudet, J. C.; Pouligny, B. How do Mosquito eggs self-assemble on the water surface? *Eur. Phys. J. E* **2011**, *34*, 1.

(31) Wang, A.; Rogers, W. B.; Manoharan, V. N. Effects of contact-line pinning on the adsorption of nonspherical colloids at liquid interfaces. *Phys. Rev. Lett.* **2017**, *119*, 108004.

(32) Coertjens, S.; De Dier, R.; Moldenaers, P.; Isa, L.; Vermant, J. Adsorption of Ellipsoidal Particles at Liquid-Liquid Interfaces. *Langmuir* **2017**, *33*, 2689−2697.

(33) Fournier, J. B.; Galatola, P. Anisotropic capillary interactions and jamming of colloidal particles trapped at a liquid-liquid interface. *Phys. Rev. E: Stat., Nonlinear, Soft Matter Phys.* **2002**, *65*, 031601.

(34) Zhang, Z.; Pfleiderer, P.; Schofield, A. B.; Clasen, C.; Vermant, J. Synthesis and directed self-assembly of patterned anisometric polymeric particles. *J. Am. Chem. Soc.* **2011**, *133*, 392−395.

DOI: 10.1021/acsomega.8b01818
ACS Omega 2018, 3, 14962−14972

(35) Zabow, G.; Dodd, S. J.; Koretsky, A. P. Ellipsoidal microcavities: electromagnetic properties, fabrication, and use as multispectral MRI agents. *Small* **2014**, *10*, 1902−1907.
(36) Hyeon, T. Chemical synthesis of magnetic nanoparticles. *Chem. Commun.* **2003**, 927−934.
(37) Li, F.; Josephson, D. P.; Stein, A. Colloidal assembly: the road from particles to colloidal molecules and crystals. *Angew. Chem. Int. Ed.* **2011**, *50*, 360−388.
(38) Anjali, T. G.; Basavaraj, M. G. Shape anisotropic colloids at interfaces. *Langmuir* **2018**, DOI: 10.1021/acs.langmuir.8b01139.
(39) Danov, K. D.; Kralchevsky, P. A.; Naydenov, B. N.; Brenn, G. Interactions between particles with an undulated contact line at a fluid interface: capillary multipoles of arbitrary order. *J. Colloid Interface Sci.* **2005**, *287*, 121−134.
(40) Stamou, D.; Duschl, C.; Johannsmann, D. Long-range attraction between colloidal spheres at the air-water interface: the consequence of an irregular meniscus. *Phys. Rev. E: Stat., Nonlinear, Soft Matter Phys.* **2000**, *62*, 5263−5272.
(41) *Structure and Functional Properties of Colloidal Systems*; Hidalgo-Álvarez, R., Ed.; CRC Press, 2009; Vol. *146*.

DOI: 10.1021/acsomega.8b01818
ACS Omega 2018, 3, 14962−14972